

Two-photon fluorescence cross-section measurements calibrated with hyper-Rayleigh scattering

Philip Kaatz and David P. Shelton

Department of Physics, University of Nevada Las Vegas, Las Vegas, Nevada 89154-4002

Received May 29, 1998; revised manuscript received September 28, 1998

The intensity of two-photon-excited fluorescence measured relative to the intensity of hyper-Rayleigh scattering in the same apparatus was used to determine the two-photon-excited fluorescence cross sections of the xanthene dyes Rhodamine B, Rhodamine 6G, and Fluorescein. The measured cross sections at $\lambda_0 = 1064$ nm are $\sigma_{2PF}^{(2)} = 1.5 \pm 0.3 \times 10^{-50}$ cm⁴ s, $2.0 \pm 0.4 \times 10^{-50}$ cm⁴ s, and $1.4 \pm 0.3 \times 10^{-52}$ cm⁴ s, for the three dyes, respectively. The two-photon-excited fluorescence cross section of Rhodamine B was also calibrated with one-photon-excited fluorescence in this apparatus. The result, $\sigma_{2PF}^{(2)} = 2.3 \pm 0.7 \times 10^{-50}$ cm⁴ s, is in reasonable agreement with the result calibrated by hyper-Rayleigh scattering. The results for Rhodamine B are 1.5–6 times smaller than previous results calibrated by one-photon-excited fluorescence. © 1999 Optical Society of America [S0740-3224(99)01406-X]

OCIS codes: 190.4180, 190.4710, 300.2530, 300.6410.

1. INTRODUCTION

There has been renewed interest in two-photon fluorescence (2PF) owing to its recent application in two-photon fluorescence microscopy,¹ as well as other emerging applications.^{2–4} Accurate absolute 2PF cross sections are needed to support the development of these applications. However, despite the long history of 2PF studies, absolute determinations of 2PF cross sections remain infrequent and difficult, and substantial disagreements between published values of 2PF cross sections often exist.^{5–7} One can determine the 2PF cross section $\sigma_{2PF}^{(2)}$ directly by measuring the fluorescence intensity. Or, one can determine it indirectly by combining a measurement of the two-photon absorption cross section mediated by $\text{Im} \chi^{(3)}$ with an estimate of the quantum efficiency η_F for subsequent fluorescence from the two-photon excited state.

Direct 2PF intensity measurements have used forward,⁸ backward,⁹ or 90° scattering geometries,^{7,10–12} with light collected over wide⁸ or narrow⁹ apertures, but in all cases the absolute calibration of the measurement has been done by comparison to one-photon fluorescence (1PF) in the same sample. The 1PF excitation source can come from a different laser,^{7,9} or it can be derived from the 2PF excitation laser by phase-matched^{8,10,11} or non-phase-matched¹² second-harmonic generation (SHG). In spite of the various innovations, a weak point in all these experiments is the calibration of 2PF in terms of 1PF. The dependence on experimental parameters is dramatically different for 1PF and 2PF, so the spatial and the temporal properties of the laser will enter the cross-section determination in more-or-less subtle ways because different light sources must be used for measure-

ment and calibration. Indirect determinations based on two-photon absorption tend to be more difficult and less reliable.

The essential feature of the method presented here is that it compares two different two-photon scattering processes in the same sample under identical conditions, in this case, 2PF and hyper-Rayleigh scattering (HRS). Although the dependence on experimental parameters of the intensity of 2PF and HRS is almost identical, the light scattered by the two processes can be readily distinguished spectroscopically. The spectrum of the light produced by HRS is sharply peaked near twice the incident-laser frequency, whereas the 2PF emission spectrum is broader and shifted to frequencies lower than the HRS spectrum. The angular, spectral, and polarization dependence of HRS is very well understood, which makes HRS a good reference. The most critical aspect is that an accurate value for the hyperpolarizability β must be available. Recent work has provided accurate HRS β values for a number of chromophores in solution.^{13–15} This makes HRS a feasible alternative to 1PF for the calibration of 2PF measurements. Xu *et al.*¹⁶ have previously compared HRS and 2PF. However, the results of that work are unsuitable for calibration purposes, as no consideration was given to the angular distribution and the polarization dependence of HRS. The following work presents several measurements of 2PF calibrated with HRS. In addition, a measurement of the 2PF signal calibrated with respect to 1PF was made to explore the relative merits of the HRS and 1PF calibration techniques. Finally, several absolute cross-section measurements were made, to better understand potential sources of systematic errors.

2. METHODS FOR THE DETERMINATION OF TWO-PHOTON-EXCITED FLUORESCENCE CROSS SECTIONS

A. Comparison of Two-Photon-Excited Fluorescence with Hyper-Rayleigh Scattering

Both 2PF and HRS are two-photon induced processes, and the description of the generated signal is similar for the two cases. The number of detected photons per laser pulse, S , owing to either 2PF or HRS is proportional to the number density of molecules ρ and to the differential scattering cross section per molecule $d^2\sigma^{(2)}/d\Omega d\omega'$ and is given by

$$S(\omega') = \rho \frac{d^2\sigma^{(2)}}{d\Omega d\omega'} \left(\frac{n_\omega \pi}{M^2 \lambda_0} \right) \left(\frac{G^{(2)} N_\omega^2}{1.64 \tau_{\text{FWHM}}} \right) \left(\frac{d\Omega}{n_{\omega'}^2} \right) \times (T_\omega^2 T_{\omega'} 10^{-2A_\omega l_1} 10^{-A_{\omega'} l_2} \eta_D), \quad (1)$$

where λ_0 is the vacuum wavelength of the incident light with frequency ω , n is the sample refractive index, N_ω is the number of photons in the laser pulse, and τ_{FWHM} is the pulse duration. The doubly differential scattering cross section in Eq. (1) is defined as the number of photons scattered per molecule per unit time into a unit solid angle and a unit frequency interval (for photons with a specified frequency, polarization, and direction), divided by the square of the incident photon flux (for an incident beam of photons with a specified frequency, polarization, and direction). In Eq. (1) the four factors in parentheses account for (i) the spatial-intensity distribution of the focused fundamental Gaussian beam; (ii) the time dependence of the pulse intensity, where the form $t \exp(-t/t_0)$ is assumed; (iii) scattered-light collection, where $d\Omega$ is the solid angle subtended by the collecting lens; and (iv) the imperfect transmission of light into and out of the sample, and the detector efficiency η_D for photons that enter the collection lens. The Fresnel transmission factors at the sample boundaries are T_ω and $T_{\omega'}$ for the incident and the scattered light, respectively.

The sample cell, the incident beam, and the scattered light are shown schematically in Fig. 1. The incident beam travels a distance l_1 to reach the focus, through the sample with absorbance A_ω , while the scattered light travels a distance l_2 to leave, through the sample with absorbance $A_{\omega'}$. Since light is scattered with a range of

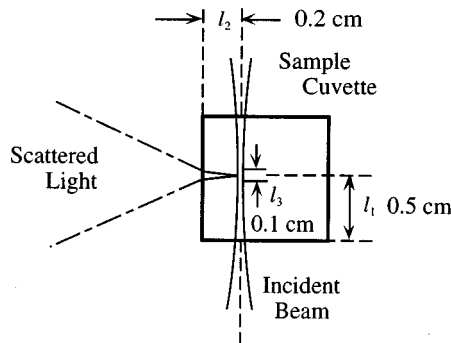


Fig. 1. Schematic diagram of the geometry of the sample cell used for the 1PF, 2PF, and HRS experiments, showing the placement of the incident laser beam with respect to the sample cell. The scattered light is detected in a solid angle $d\Omega = 0.18$ sr subtended by the camera lens at 90° to the incident beam.

frequencies near 2ω , the spectral variation of the instrumental factors over the scattered spectrum must be considered. Beam aberrations are accounted for by the space-bandwidth product $M^2 \geq 1$, while the coherence function $G^{(2)}$ accounts for the temporal fluctuations superimposed on the pulse envelope by the mode structure of the laser. For a pulse whose envelope varies slowly compared with the mode-beating noise, $G^{(2)} = \langle I^2 \rangle / \langle I \rangle^2$ and $1 \leq G^{(2)} \leq 2$, where the average is taken over a time short compared with the pulse length but long compared with the fluctuations.

The total 2PF cross section $\sigma_{2\text{PF}}^{(2)}$ is the photon-scattering rate, R , per molecule, divided by the incident flux, F , squared,

$$\sigma_{2\text{PF}}^{(2)} = \frac{R}{F^2}, \quad (2)$$

including scattered photons of all frequencies, all directions, and both polarizations. In the case of unpolarized, isotropic fluorescence, the total 2PF cross section is given in terms of the differential cross section by

$$\sigma_{2\text{PF}}^{(2)} = 2 \times 4\pi \times \frac{d\sigma_{2\text{PF}}^{(2)}}{d\Omega}, \quad (3)$$

where the differential cross section integrated over the scattered spectrum can be obtained from the measured signal obtained by Eq. (1). An accurate evaluation of all the factors in Eq. (1) is difficult, but most of the difficulties can be avoided by use of the HRS cross section for calibration. The only measurement that is needed to determine the 2PF cross section calibrated in terms of the HRS cross section is the relative integrated intensity of the 2PF and the HRS components of the scattered-light spectrum (corrected for the relative spectral response of the detector and absorption of the scattered light by the sample). All other factors in Eq. (1) cancel out, and one has the simple expression

$$\sigma_{2\text{PF}}^{(2)} = 8\pi \frac{S_{2\text{PF}}^*}{S_{\text{HRS}}^*} \frac{d\sigma_{\text{HRS}}^{(2)}}{d\Omega}, \quad (4)$$

where

$$S^* = \frac{1}{\rho} \int \frac{S(\omega') d\omega'}{10^{-A(\omega') l_2} \eta_D(\omega')} \quad (5)$$

is the integrated intensity per molecule after correction for reabsorption of scattered light by the sample and the relative spectral response of the spectrometer. The relative spectral response of the spectrometer is measured with a calibrated quartz-tungsten-halogen lamp, and the sample spectral absorbance is measured with a standard spectrophotometer. The expression for the HRS cross section in the 90° scattering geometry, with both incident and scattered light polarized perpendicular to the scattering plane (VV polarization), is given by

$$\frac{d\sigma_{\text{HRS}}^{(2)}}{d\Omega} = \frac{2h}{(4\pi\epsilon_0)^3} \left(\frac{2\pi}{\lambda_0} \right)^5 L_\omega^4 L_{2\omega}^2 \langle \beta_{\text{ZZZ}}^2 \rangle, \quad (6)$$

where $L = (n^2 + 2)/3$ is the Lorentz local-field factor, β is defined by the convention $\mu = 1/2K\beta E^2$, where K

= 1/2 for SHG, and $\langle \beta_{zzz}^2 \rangle$ is the Z (parallel) component of the orientationally averaged β^2 tensor.¹⁷ It is straightforward to generalize Eq. (4) to the case where the 2PF and HRS measurements are made on different samples in the same apparatus.¹⁴ Equation (4) remains correct as written if all samples use the same solvent and if the chromophores are sufficiently dilute. The calibration of the HRS standard is outlined in Appendix A.

B. Comparison of Two-Photon-Excited Fluorescence with One-Photon-Excited Fluorescence

As discussed in the introduction, in all previous work the calibration of two-photon-induced fluorescence from organic dyes has been done with respect to the fluorescence excited by one-photon absorption. The number of detected photons owing to 1PF, S_{1PF} , in our experimental geometry is given by

$$S_{1PF}(\omega') = N_{2\omega}(1 - 10^{-A_{2\omega}l_3}) \left[\frac{\eta_F g(\omega')}{2 \times 4\pi} \right] \left(\frac{d\Omega}{n_{\omega'}^2} \right) \times (T_{2\omega} T_{\omega'} 10^{-A_{2\omega}l_4} 10^{-A_{\omega'}l_2} \eta_D), \quad (7)$$

where $N_{2\omega}$ is the number of photons per pulse in the incident second-harmonic laser beam. The factor in the first parentheses accounts for the fraction of light with frequency 2ω absorbed in the length l_3 , where l_3 is the effective sample length determined by the spectrometer slit length and the magnification of the collection optics. In the next factor in square brackets, η_F is the fluorescence quantum efficiency for an excited molecule, $g(\omega')$ is the normalized fluorescence spectral distribution function, and $2 \times 4\pi$ in the denominator accounts for a single detected polarization of the light scattered into 4π sr. The remaining factors in parentheses in Eq. (7) account for (i) scattered-light collection, where $d\Omega$ is the solid angle subtended by the collecting lens, and (ii) the imperfect transmission of light into and out of the sample and the detector efficiency η_D for photons that enter the collection lens. The final factor differs from that in Eq. (1) in that it is linear in the corrections affecting the incident-beam intensity, where the Fresnel transmission factor is $T_{2\omega}$ at the input sample boundary, the absorbance for the incident beam is given by $A_{2\omega}$, and $l_4 = l_1 - 1/2 l_3$ is the distance to the beginning of the scattering source region.

The two-photon fluorescence cross section $\sigma_{2PF}^{(2)}$ is obtained from measurements of S_{2PF}^* and S_{1PF}^* by use of Eqs. (1), (3), (5), and (7). In contrast to the calibration of 2PF cross sections by HRS, calibration of 2PF cross sections with respect to 1PF also requires knowledge of the spatial- and temporal-mode structure of the laser beam used for two-photon excitation as well as most of the other experimental factors present in Eqs. (1) and (7).

C. Absolute Cross-Section Determinations

The information needed to make an absolute determination of the scattering cross section from Eq. (1), in addition to the laser-beam parameters, is the value of the product $d\Omega \eta_D$, which characterizes the collection optics and the spectrometer. We obtained the value $d\Omega = 0.18$ sr by measuring the scattered light signal as a

function of the f -stop setting of the collecting lens. We measured the value $\eta_D = 0.0095$ at $\lambda = 632.8$ nm by sending an attenuated, collimated He-Ne laser beam through the spectrometer slit and measuring the photon count rate. These values for $d\Omega$ and η_D agree with rough estimates based on the geometry and properties of the various components of the apparatus, and they serve as a good check for gross errors. However, it is more accurate to measure the collection angle-detection efficiency product with a calibrated scatter plate. This was done with a target of Spectralon (a material with high white-diffuse reflectance)¹⁸ placed at the sample position and illuminated with a He-Ne laser beam focused by the same lens used in the 1PF, 2PF, and HRS measurements. The image of the focused spot formed by the collection optics is small compared with the width of the spectrometer entrance slit, so all of the collected light enters the spectrometer. The collection geometry and the spectrometer illumination conditions during calibration reproduce the conditions of the 2PF measurements.

An integrating sphere is used to calibrate the scattering cross section of the scatter plate. The scatter plate is calibrated and used with the laser beam incident at 45° . The differential cross section is obtained from the ratio of the signal with the integrating sphere collecting scattered light to the signal from the integrating sphere collecting the entire incident laser beam. The relevant solid angle is given by the area of the circular entrance aperture of the integrating sphere divided by the square of the distance between the entrance aperture and the source spot. Measurements were made at several distances such that the solid angle of the collection optics was bracketed. Deviations from uniformity owing to the $\cos^2 \theta$ variation of HRS and $\cos \theta$ variation of Lambertian scattering sources over 0.2 sr had an insignificant effect on the calibrations.

The result of calibrating the spectrometer collection angle and the detection efficiency product with the scatter plate is $d\Omega \eta_D = 8.5 \pm 0.4 \times 10^{-4}$ sr at $\lambda = 632.8$ nm. We obtained the absolute spectrometer calibration at other wavelengths by combining the absolute calibration at 632.8 nm with the relative spectral response of the spectrometer measured with a calibrated quartz-tungsten-halogen lamp. This gives $d\Omega \eta_D = 1.61 \pm 0.08 \times 10^{-3}$ sr at $\lambda = 532$ nm, for example. Because the spectrometer absolute calibration uncertainty has been reduced to only $\pm 5\%$, the accuracy of absolute cross-section determinations is controlled by the uncertainties of the laser parameters. Therefore the absolute cross section determined directly from Eq. (1) should be just as accurate as the cross section calibrated with 1PF.

3. EXPERIMENT

The calibration of 2PF by HRS with Eqs. (4) and (6) was applied to the measurement of $\sigma_{2PF}^{(2)}$ for the well-studied xanthene dyes Rhodamine B (RhB), Rhodamine 6G (Rh6G), and Fluorescein, using the apparatus that has been described in previous publications.^{13,14} Light pulses from an acousto-optically Q -switched Nd:YAG laser (Quantronix 116) at $\lambda_0 = 1064$ nm were focused into the sample contained in a 1-cm cuvette, and the photons scattered at 90° were collected and detected. The effec-

tive scattering source is approximately a cylinder with dimensions of 11- μm diameter by 110- μm length, located 2 mm behind the cell window. Pulses with $\tau_{\text{FWHM}} = 125$ ns and energies up to 60 μJ were used, giving peak incident photon fluxes up to $F = 3 \times 10^{27}$ photons $\text{cm}^{-2} \text{s}^{-1}$. Both HRS and 2PF processes showed the expected quadratic dependence on the incident photon flux, as indicated in Fig. 2.

The 2PF from each of the three dyes dissolved in methanol-*d* was compared with the HRS from *p*-nitroaniline (*p*NA), also in methanol-*d*. The Fluorescein solution was made basic with the addition of a small amount of sodium hydroxide to ensure that the dye was deprotonated. The solutions were sufficiently dilute that the corrections for reabsorption of scattered light were small, 2% for RhB and Rh6G, 10% for Fluorescein, and 0% for *p*NA. Rhodamine B and *p*NA spectra, corrected for the relative spectral response of the apparatus and reabsorption, are shown in Fig. 3. The spectra of Rh6G and Fluorescein are similar except for an overall shift of the spectra to higher frequencies. Since the RhB fluorescence band is narrow and almost overlaps the HRS spectrum, the spectral response correction to the ratio of integrated intensities is not large ($1.15\times$). However, as 2PF is much stronger than HRS in this case, some care is necessary to maintain an adequate HRS signal while saturation of the detector with the 2PF signal is avoided (the maximum dead time correction is 15%).

To calibrate the 2PF coefficient by 1PF, the same laser system was also used to generate light at 2ω by SHG in a KTP crystal. The photon fluxes of the incident beams at ω and 2ω used to generate 2PF and 1PF, respectively, were measured and cross calibrated with several photoelectric and thermal powermeters. The spatial-mode structure of the laser beam at ω , as characterized by the

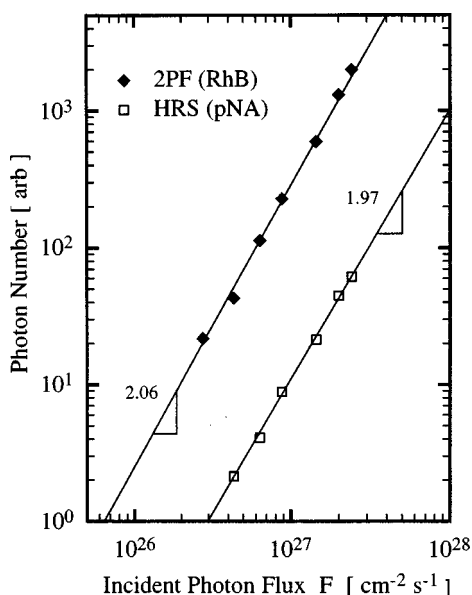


Fig. 2. Nearly quadratic power dependence is observed over the range of incident photon fluxes used for the measurements of HRS from a 0.096 M solution of *p*-nitroaniline (*p*NA) in methanol-*d*, and for measurements of 2PF from a 2.92×10^{-6} M solution of Rhodamine B (RhB), also in methanol-*d*. The results for Rhodamine 6G and Fluorescein are similar.

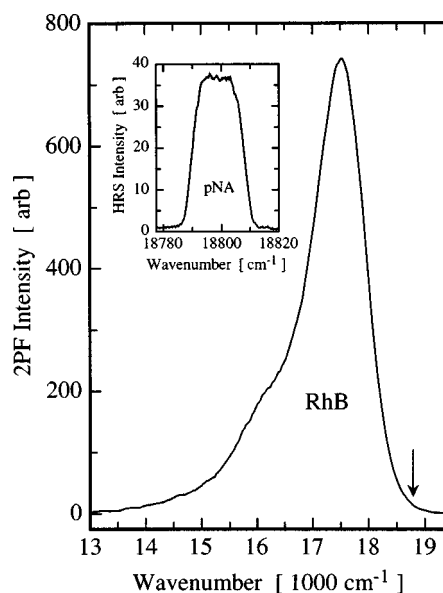


Fig. 3. 2PF spectrum of a 2.92×10^{-6} M solution of Rhodamine B (RhB) in methanol-*d* compared with the HRS spectrum (inset) of a 0.096 M solution of *p*-nitroaniline (*p*NA) also in methanol-*d* used for calibration. Both spectra were obtained in the VV polarization geometry with an 18- cm^{-1} spectral slit width. The arrow marks the position of the RhB HRS peak, which is too narrow and too weak to be seen on this scale.

beam-propagation parameter M^2 , was measured by a moving knife edge and had the value of $M^2 = 1.21 \pm 0.04$. The envelope of the laser pulse was measured with a fast photodiode and a transient digitizer with a 1-GHz bandwidth. The temporal intensity fluctuations around the envelope were measured with a second-harmonic autocorrelator, giving the value $G^{(2)} = 1.99 \pm 0.03$. The measured SHG autocorrelation trace was consistent with the measured 0.7- cm^{-1} spectral bandwidth of the Quantronix laser source. This bandwidth supports $m = 100$ simultaneously oscillating longitudinal modes, which is consistent with $G^{(2)} = 2 - m^{-1} = 1.99$.

4. RESULTS AND DISCUSSION

A. Hyper-Rayleigh Scattering and One-Photon-Excited Fluorescence Calibration Results

The HRS calibration data for *p*NA is given in Table 1. The data used to obtain $\sigma_{2\text{PF}}^{(2)}$ for the xanthene dyes is given in Table 2 along with the two-photon fluorescence and absorption cross sections obtained in this work by HRS calibration. The two-photon absorption coefficient, δ , is evaluated to facilitate comparison with the results of previous work. The cross section δ is the photon-absorption rate, R' , per molecule divided by the incident flux, F , squared, $\delta = R'/F^2$. With this definition,

$$\delta = 2 \left(\frac{\sigma_{2\text{PF}}^{(2)}}{\eta_F} \right), \quad (8)$$

where the factor 2 accounts for two photons absorbed for each excited molecule produced, and the fluorescence quantum efficiency η_F is assumed to be the same for both one- and two-photon processes. In Tables 3–5 the results of the present work are compared with previous measure-

ments of δ for RhB, Rh6G, and Fluorescein, respectively, at or near 1064 nm. The results for RhB are also compared graphically in Fig. 4. Some authors define δ in terms of the molecular-excitation rate rather than the photon-absorption rate. Their δ values are multiplied by 2 to make them comparable (in some cases it is uncertain which definition was actually followed). The present results differ from the previous results by factors of 0.9–12.

In an attempt to resolve these discrepancies, we have first reconsidered the assumptions entering the analysis of the present experiment. Unpolarized isotropic fluorescence is expected if collisions reorient the chromophore on a time scale short compared with the fluorescence lifetime. This assumption was tested with measurements of the scattered intensity for various combinations of incident and scattered polarization. The measurements are consistent with unpolarized, isotropic fluorescence. Normalized to the integrated intensity for VV polarization, the measured and predicted intensities for RhB are (VV, HV, VH, HH) = (1.00, 0.99, 1.00, 1.01) measured and (1.00, 1.00, 1.00, 1.00) predicted.

Stimulated emission depletes the excited-state population, reducing the 2PF signal at 90° by the factor $(1 + \tau_F \sigma F)^{-1}$, where the fluorescence decay time is $\tau_F = 3$ ns at 300 K for RhB.¹⁹ The emission cross section at 1064 nm would have to be at least 10^{-19} cm² for there to be a significant effect owing to stimulated-emission quenching of the fluorescence, whereas the estimated cross section is 10^{-21} cm².¹⁹ The observed quadratic laser-power dependence of the 2PF and HRS intensities also argues against a significant quenching effect.

We also calibrated the 2PF cross section using 1PF in the present apparatus, giving $\delta = 6.8 \pm 2.1 \times 10^{-50}$ cm⁴ s for RhB. This result is 1.5 times larger than the 2PF result calibrated with HRS. The error bar includes the uncertainties in the experimental parameters characterizing the apparatus that appear in Eq. (1), as well as additional uncertainties associated with the different effective source geometries for 2PF and 1PF.

Table 1. Hyper-Rayleigh-Scattering Calibration Data for Para-Nitroaniline (pNA) in Methanol-*d* at $\lambda_0 = 1064$ nm

Material	Quantity	Value
CH ₃ OD	n_ω	1.322
	$n_{2\omega}$	1.330
pNA/CH ₃ OD	ρ_{pNA}	0.096 M
	$\langle \beta_{zzz}^2 \rangle^{1/2}$	$5.65 \pm 0.23 \times 10^{-50}$ C ³ m ³ J ⁻²
	$d\sigma_{\text{HRS}}^{(2)}/d\Omega$	$8.5 \pm 0.7 \times 10^{-60}$ cm ⁴ s sr ⁻¹

Table 2. Data Used to Obtain $\sigma_{2\text{PF}}^{(2)}$ and δ for Each Dye—All Dyes Were Studied as Solutions in CH₃OD—NaOH Was Added to Give a pH \approx 10 for the Fluorescein Solution

Material	$S_{2\text{PF}}^*/S_{\text{HRS}}^*$	ρ [M]	$\sigma_{2\text{PF}}^{(2)}$ [10^{-50} cm ⁴ s]	η_F	δ [10^{-50} cm ⁴ s]
RhB	$7.2 \pm 0.7 \times 10^7$	2.96×10^{-6}	1.5 ± 0.3	0.67 ± 0.05^a	4.6 ± 0.9
Rh6G	$9.4 \pm 0.9 \times 10^7$	2.17×10^{-6}	2.0 ± 0.4	0.95 ± 0.05^a	4.2 ± 0.8
Fluorescein	$6.8 \pm 0.7 \times 10^5$	2.07×10^{-5}	0.014 ± 0.003	0.90 ± 0.05^a	0.032 ± 0.006

^aJ. N. Demas and G. A. Crosby, "The measurement of photoluminescence quantum yields: a review," J. Phys. Chem. **75**, 991–1024 (1971).

The present results calibrated by HRS and 1PF are in reasonable agreement with each other, but both disagree with the previous results.

B. Absolute Cross-Section Results

The intent of the HRS calibration is to make the 2PF cross-section results insensitive to laser parameters that are difficult to accurately characterize and control. Since there is a large discrepancy with previous results, one needs to test for systematic errors. A way to test the theoretical expressions and experimental methods is to make absolute cross-section measurements for several different linear and nonlinear scattering processes. Absolute cross-section determinations are sensitive to all experimental parameters, so systematic errors can be revealed by comparing observed and predicted signals.

Absolute cross sections were measured for two linear-scattering processes (rotational Raman scattering and 1PF) and two nonlinear scattering processes (HRS and 2PF). Expressions have already been given for the HRS, 2PF, and 1PF signals. The corresponding expression for the Raman-scattering signal, S_{RS} , is

$$S_{\text{RS}}(\omega') = N_\omega \rho l_3 \frac{d\sigma_{\text{RS}}}{d\Omega} d\Omega T_\omega T_{\omega'} \eta_D, \quad (9)$$

where N_ω is the number of photons per pulse in the incident laser beam and ρ is the molecular density. The expression for the cross section $d\sigma_{\text{RS}}/d\Omega$ for the $S(J)$ rotational Raman line of a linear rotor, observed in the VV polarization geometry, is^{20–22}

$$\frac{d\sigma_{\text{RS}}}{d\Omega} = \rho(J) \frac{\omega \omega'^3}{c^4} \frac{4}{45} \frac{3}{2} \frac{(J+1)}{(2J+1)} \frac{(J+2)}{(2J+3)} \frac{|\Delta\alpha|^2}{(4\pi\epsilon_0)^2}, \quad (10)$$

where $\rho(J)$ is the fraction of the molecules in the initial J th rotational level and $\Delta\alpha$ is the transition polarizability anisotropy of the molecule. The $S(1)$ rotational Raman line was measured for a gas-phase H₂ sample, excited at 514.5 nm with a cw argon-ion laser beam, with scattered light collected at $\nu' = 18849$ cm⁻¹ (Raman shift 587 cm⁻¹). At 295 K, $\rho(1) = 0.6667$ for H₂. The value of the transition polarizability anisotropy at 514.5 nm is $\Delta\alpha = 2.1546$ au = 1.8267×10^{-29} C² m² J⁻¹ for the $v, J = 0, 1 \rightarrow 0, 3$ transition in H₂, obtained with high accuracy from the *ab initio* calculations of Bishop and Pipin.²³

The measured and predicted Raman, 1PF, 2PF, and HRS signals are compared in Table 6. In each case the predicted signal is based on an independently determined molecular polarizability, hyperpolarizability, or absorbance, combined with measurements of laser-beam, sample, and spectrometer parameters. The measured

Table 3. Comparison of Measurements of the Two-Photon Absorption Cross Section δ of Rhodamine B—All These Experiments Actually Measure the 2PF Cross Section Divided by the Fluorescence Quantum Efficiency η_F to Obtain the 2PA Coefficient δ

Solvent	Concentration [M]	Pulse	Wavelength [nm]	Calibration Method/Geometry	δ [$10^{-50} \text{ cm}^4 \text{ s}$]	δ [$10^{-50} \text{ cm}^4 \text{ s}$] ^a	Reference
CH ₃ OD	$2.92 \cdot 10^{-6}$	125 ns	1064	HRS/90°	4.6 ± 0.9		This work
CH ₃ OD	$2.52 \cdot 10^{-6}$	125 ns	1064	1PF/90°	6.8 ± 2.1		This work
CH ₃ OD	$2.52 \cdot 10^{-6}$	125 ns	1064	Absolute/90°	6.4 ± 1.7		This work
CH ₃ OH	10^{-4}	100 fs	1050	1PF/180°	20 ± 6	10 ± 5^b	Xu (1996)
C ₂ H ₅ OH	10^{-6}	110 ns	1064	1PF/90°	24 ± 12^c	12 ± 5^d	Li (1982)
n.a. ^e	10^{-2}	cw	1064	1PF/0°	26 ± 5^e	13 ± 3^d	Catalano (1981)
C ₂ H ₄ Cl ₂	10^{-5}	ps	1060	1PF/90°	7	7	Bradley (1972)
C ₂ H ₄ Cl ₂	10^{-5}	ns	1060	1PF/90°	14	7^d	Bradley (1972)
C ₂ H ₅ OH	n.a. ^e	ns	1060	1PF/90°	28 ± 14^c	11 ± 6^f	Hermann (1972)

^a Reevaluated by the present authors.

^b Obtained by extrapolation of the excitation spectrum in Fig. 2 of Ref. 9 from 1050 nm to 1064 nm.

^c Published values are multiplied by 2 to conform with the definition of δ in Eq. (8); see text.

^d Reevaluated assuming $G^{(2)} = 2.0$; see text.

^e Not available.

^f Reevaluated with the current reference value of quartz, $d_{11} = 0.30 \text{ pm/V}$ (from 0.48 pm/V); see text.

Table 4. Comparison of Measurements of the Two-Photon Absorption Cross Section δ of Rhodamine 6G

Solvent	Concentration [M]	Pulse	Wavelength [nm]	Calibration Method/Geometry	δ [$10^{-50} \text{ cm}^4 \text{ s}$]	δ [$10^{-50} \text{ cm}^4 \text{ s}$] ^a	Reference
CH ₃ OD	$2.17 \cdot 10^{-6}$	125 ns	1064	HRS/90°	4.2 ± 0.8		This work
C ₂ H ₅ OH	10^{-6}	110 ns	1064	1PF/90°	11 ± 5^b	5.5 ± 2.5^c	Li (1982)
C ₂ H ₅ OH	10^{-4}	30 ns	1060	1PF/90°	52^b	26^c	Vsevolodov (1973)
C ₂ H ₅ OH	10^{-5}	ps	1060	1PF/90°	3.6	3.6	Bradley (1972)
C ₂ H ₅ OH	10^{-5}	ns	1060	1PF/90°	5.5	2.8^c	Bradley (1972)
C ₂ H ₅ OH	n.a. ^d	ns	1060	1PF/90°	26 ± 12^b	10 ± 5^e	Hermann (1972)

^a Reevaluated by the present authors.

^b Published values are multiplied by 2 to conform with the definition of δ in Eq. (8); see text.

^c Reevaluated assuming $G^{(2)} = 2.0$; see text.

^d Not available.

^e Reevaluated with the current reference value of quartz, $d_{11} = 0.30 \text{ pm/V}$ (from 0.48 pm/V); see text.

Table 5. Comparison of Measurements of the Two-Photon Absorption Cross Section δ of Fluorescein

Solvent	Concentration [M]	Pulse	Wavelength [nm]	Calibration Method/Geometry	δ [$10^{-52} \text{ cm}^4 \text{ s}$]	δ [$10^{-52} \text{ cm}^4 \text{ s}$] ^a	Reference
CH ₃ OD pH 10	$2.07 \cdot 10^{-5}$	125 ns	1064	HRS/90°	3.2 ± 0.6		This work
H ₂ O pH 11	$8 \cdot 10^{-5}$	100 fs	1050	1PF/180°	23 ± 7		Xu (1996)
C ₂ H ₅ OH	10^{-5}	ps	1060	1PF/90°	7.5	7.5	Bradley (1972)
C ₂ H ₅ OH	10^{-5}	ns	1060	1PF/90°	18	9^b	Bradley (1972)

^a Reevaluated by the present authors.

^b Reevaluated assuming $G^{(2)} = 2.0$; see text.

signals tend to be larger than predicted, especially for the nonlinear optical processes, but this tendency falls within the range allowed by calibration uncertainties for the measuring instruments (e.g., optical powermeters). There is no evidence for unanticipated systematic errors in the experiment.

The 2PA coefficient δ obtained for RhB with the absolute calibration method is shown in Table 3. Compared with HRS calibration, the absolute cross-section determination requires many additional difficult supplementary measurements and gives an error bar almost twice as

large. The results for δ with HRS, 1PF, and absolute calibration show no significant disagreement.

C. Reappraisal of Previous Results

The discrepancies between the results of this work and the previous 2PF results may be caused by inadequate measurements or incomplete analysis in the the previous work. Previously demonstrated sources of systematic errors in nonlinear optical experiments include spatial and temporal fluctuations of the laser beam²⁴ and multiple-

reflection effects in the sample.²⁵ Using the published descriptions of the 2PF experiments, we attempted to identify sources of systematic errors and to reassess the previous results for δ . In one case the source of the disagreement is clear. The measurement of Hermann and Ducuing¹² was calibrated with SHG from quartz assuming a nonlinear optical coefficient $d_{11} = 0.48$ pm/V.⁵ Substituting the currently accepted value²⁵⁻²⁷ for quartz, $d_{11} = 0.30$ pm/V, reduces their value for the two-photon absorption cross section of Rhodamine B to $\delta = 11 \pm 6 \times 10^{-50}$ cm⁴ s, which is in fair agreement with the best result obtained in this work by HRS calibration, $\delta = 4.6 \pm 0.9 \times 10^{-50}$ cm⁴ s. Fair agreement is also obtained with the reanalyzed result for Rh6G (see Table 4). Note that the results of Hermann and Ducuing should be only weakly sensitive to the effects of spatial and temporal fluctuations of the laser beam, since the SHG beam intensity was obtained in terms of the fundamental beam intensity and d_{11} for quartz.

A different systematic error is readily apparent in several of the other previous 2PF experiments that used SHG to produce the light for 1PF calibration. In those experiments the fundamental and harmonic beam intensities were independently measured; thus the effects of spatial and temporal fluctuations of the laser beam did not cancel out in their final results. For the typical cw- and ns-pulse Nd:YAG lasers such as used by Catalano,⁸ Li,¹⁰ Bradley,¹¹ and Vsevolodov,²⁸ mode-beating noise gives $G^{(2)} = 2.0$ (whereas for mode-locked pulses $G^{(2)} = 1.0$). Since $G^{(2)}$ was not included in the analysis of these experiments, their results for δ are too large by a factor of 2. Accounting for this factor, the results of

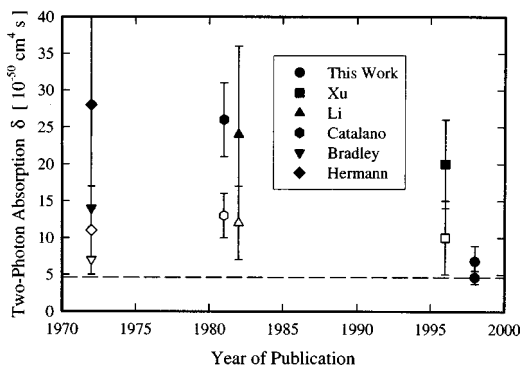


Fig. 4. Measured values of the two-photon absorption coefficient δ of RhB plotted versus the year the work was reported. Solid symbols correspond to the original data as given in Table 3, whereas the open symbols indicate the values as reassessed by the present authors (also given in Table 3). The dashed line indicates the best present estimate for δ of RhB.

Table 6. Absolute Intensity Measurements Compared with Predictions

Scattering Process	Sample	Measured/Predicted Signal
Raman	H ₂	1.20 ± 0.26
1PF	RhB/MeOD	0.95 ± 0.20
2PF	RhB/MeOD	1.39 ± 0.46 ^a
HRS	CCl ₄	1.54 ± 0.45

^a Predicted signal calculated assuming $\delta = 4.6 \pm 0.9 \times 10^{-50}$ cm⁴ s.

Catalano, Li, and Bradley fall into fair agreement with the results of the present work (see Tables 3, 4, and 5, and Fig. 4).

The discrepancy between the present results for RhB and the result of Xu⁹ is largely caused by the measurement wavelength difference. Extrapolation of their excitation spectrum from 1050 to 1064 nm gives $\delta = 10 \pm 5 \times 10^{-50}$ cm⁴ s, in fair agreement with the present results for RhB. For Fluorescein, at least part of the difference between the present result and the result of Xu is caused by spectral variation of δ , but in this case the published excitation spectrum of Fluorescein cannot be reliably extrapolated. Since δ is a strong function of wavelength, the wide spectral bandwidth of femtosecond pulses may also result in significant systematic changes in δ . Spectral variation of δ can also account for part of the difference between the results measured at 1060 and 1064 nm.

Other systematic errors can arise from the sensitivity of the 2PF intensity to spatial nonuniformities (hot spots) in the intensity of the laser beam. Hot spots can result in δ being overestimated by a large factor, but it is not possible to make an accurate estimate from the published results. Another possible systematic error may affect the work of Catalano.⁸ To spatially localize the 1PF source, they used a high dye concentration, giving an absorption length of ~ 8 μ m, comparable to the 5- μ m confocal parameter of the tightly focused laser beam. Because of the intense reabsorption of the forward scattered light by the concentrated dye solution, positioning the beam focus just 5 μ m from the desired position centered on the entrance face of the sample cell increases the 2PF light by a factor of 2 compared with the 1PF light, which travels a longer path to leave the sample, resulting in a measured value of δ that is also overestimated by a factor of ~ 2 . Again, an accurate assessment of the actual systematic error is not possible from the published results.

The reevaluated results of previous work are larger than the present results by a factor of 2 on average. This discrepancy is larger than the assigned error bars but could be accounted for by recognized systematic errors in the previous work that we cannot quantitatively assess.

5. CONCLUSIONS

The measurement of two-photon fluorescence cross sections with hyper-Rayleigh scattering for calibration is simple, and the results should be accurate. Whereas the usual 1PF calibration technique is sensitive to the temporal and spatial laser-mode structure and the sample geometry, the HRS calibration method is not. Therefore the HRS calibration method is immune to the worst of the usual systematic errors in nonlinear cross-section measurements and should be particularly useful for calibration of 2PF standards. The discrepancies between the present and previous 2PA values can be reconciled in terms of readily identified systematic errors.

APPENDIX A: BASIS FOR THE HYPER-RAYLEIGH SCATTERING CALIBRATION

An accurate HRS standard is critical for the successful application of the method in Subsection 2.A. The HRS

scattering cross section of para-nitroaniline (*p*NA) in methanol-*d* solution has been determined with an uncertainty of $\pm 8\%$ through a chain of nonlinear optical experiments. Each link in the chain leading to the HRS standard, and its contribution to the error budget, is briefly described below.

The ultimate basis for the HRS calibration is the calculated second hyperpolarizability γ of the He atom. *Ab initio* quantum-chemical calculations for two-electron atoms can be essentially exact, and Bishop's results for γ of the He atom are thought to have an accuracy better than 0.1%.²⁹ These theoretical results for helium have been used to calibrate measurements of γ for a number of small centrosymmetric molecules with gas-phase electric-field-induced second-harmonic-generation (EFISH) experiments, with typical experimental accuracy of 1%.³⁰ For γ of He and H₂, the agreement between experiment and theory has been tested at the 0.1% level.^{31,32} N₂ calibrated against He serves as a convenient secondary standard of γ with accuracy better than 1% for gas-phase EFISH measurements.³⁰

The second link in the chain is the recent gas-phase EFISH experiment that measured the first hyperpolarizabilities β at $\lambda = 1064$ nm for a number of small molecules with γ of N₂ for calibration.¹⁵ Measurement of $\gamma + \mu\beta/3kT$ over a temperature range allows both β and γ to be obtained, and such gas-phase EFISH measurements of β typically agree with *ab initio* calculations for small molecules to within 10%.^{15,32-34} The EFISH measurements of β used here have uncertainties of $\pm 5\%$.

The third link in the chain is the theoretical relation between the gas-phase HRS β and the gas-phase EFISH β . In the case that a single tensor component dominates β , the HRS and the EFISH β 's are related by a multiplicative factor insensitive to the details of the β tensor. For the molecules considered, this step does not significantly increase the uncertainty of the HRS β .¹⁵ The uncertainties in the gas-phase HRS cross sections calculated with these β 's in Eq. (6) are $\pm 10\%$.

The fourth link in the chain is the measurement of the relative intensities of HRS from gas and liquid samples of the same molecules. This gives the liquid HRS scattering cross sections calibrated in terms of the gas-phase β 's. Independent liquid HRS scattering cross-section determinations were made for six different molecules.¹⁵ At this point the uncertainty has increased to ± 15 – 25% for each cross section.

The fifth link in the chain is the determination of the liquid CCl₄ HRS cross section calibrated with the results for all six molecules in the previous step.¹⁵ This step tests self-consistency of the results and reduces statistical uncertainty by averaging. The liquid HRS cross section obtained for CCl₄ has an uncertainty of $\pm 7\%$.

The final link in the chain is the calibration of the *p*NA secondary HRS standard with liquid CCl₄ as the reference. This is done by comparison of the HRS intensities from the two samples in the same apparatus. The final result has an uncertainty of $\pm 8\%$.

The first three links in the calibration chain are forged by gas-phase EFISH measurements of β and γ with well-established reliability, while the last three links depend only on photometric comparisons. At every stage, quan-

ties with the same dependence on experimental parameters are compared in the same apparatus. While it is convenient to express the final HRS calibration result as the value of effective β for *p*NA in solution, the accuracy of the liquid HRS cross-section calibration is not affected by incomplete understanding of local-field factors and the effects of intermolecular interactions and orientational correlations in the liquid, which increase or decrease the effective β for some molecules by up to a factor of 2. This is because the directly measured quantity is the scattering cross section, and the effective β given in Table 1 is defined by Eq. (6).

REFERENCES

1. W. Denk, J. H. Strickler, and W. W. Webb, "Two-photon laser scanning fluorescence microscopy," *Science* **248**, 73–76 (1990).
2. S. Marou, O. Nakamura, and S. Kawata, "Three-dimensional microfabrication with two-photon-absorbed photopolymerization," *Opt. Lett.* **22**, 132–134 (1997).
3. G. S. He, G. C. Xu, P. N. Prasad, B. Reinhardt, J. C. Bhatt, and A. G. Dillard, "Two-photon absorption and optical-limiting properties of novel organic compounds," *Opt. Lett.* **20**, 435–437 (1995).
4. M. Cha, W. E. Torruellas, G. I. Stegeman, W. H. G. Horsthuis, G. R. Möhlmann, and J. Meth, "Two photon absorption of di-alkyl-amino-nitro-stilbene side chain polymer," *Appl. Phys. Lett.* **65**, 2648–2650 (1994).
5. J. P. Hermann and J. Ducuing, "Absolute measurement of two-photon cross sections," *Phys. Rev. A* **5**, 2557–2568 (1972).
6. W. L. Smith, "Two-photon absorption in condensed media," in *CRC Handbook of Laser Science and Technology. III. Optical Materials: Part 1*, M. J. Weber, ed. (CRC, Boca Raton, Fla., 1986), p. 229–258.
7. A. Fischer, C. Cremer, and E. H. K. Stelzer, "Fluorescence of coumarins and xanthenes after two-photon absorption with a pulsed titanium-sapphire laser," *Appl. Opt.* **34**, 1989–2003 (1995).
8. I. M. Catalano and A. Cingolani, "Absolute two-photon fluorescence with low-power lasers," *Appl. Phys. Lett.* **38**, 745–747 (1981).
9. C. Xu and W. W. Webb, "Measurement of two-photon excitation cross sections of molecular fluorophores with data from 690 to 1050 nm," *J. Opt. Soc. Am. B* **13**, 481–491 (1996).
10. S. Li and C. Y. She, "Two-photon absorption cross-section measurements in common laser dyes at 1064 μm ," *Opt. Acta* **29**, 281–287 (1982).
11. D. J. Bradley, M. H. R. Hutchinson, and H. Koetser, "Interactions of picosecond laser pulses with organic molecules. II. Two-photon absorption cross sections," *Proc. R. Soc. London, Ser. A* **329**, 105–119 (1972).
12. J. P. Hermann and J. Ducuing, "Dispersion of the two-photon cross section in rhodamine dyes," *Opt. Commun.* **6**, 101–105 (1972).
13. P. Kaatz and D. P. Shelton, "Polarized hyper-Rayleigh light scattering measurements of nonlinear optical chromophores," *J. Chem. Phys.* **105**, 3918–3929 (1996).
14. P. Kaatz and D. P. Shelton, "Spectral measurements of hyper-Rayleigh light scattering," *Rev. Sci. Instrum.* **67**, 1438–1444 (1996).
15. P. Kaatz, E. A. Donley, and D. P. Shelton, "A comparison of molecular hyperpolarizabilities from gas and liquid phase measurements," *J. Chem. Phys.* **108**, 849–856 (1998).
16. C. Xu, J. B. Shear, and W. W. Webb, "Hyper-Rayleigh and hyper-Raman scattering background of liquid water in two-photon excited fluorescence detection," *Anal. Chem.* **69**, 1285–1287 (1997).

17. R. Bersohn, Y. H. Pao, and H. L. Frisch, "Double-quantum light scattering by molecules," *J. Chem. Phys.* **45**, 3184–3198 (1966).
18. D. A. Haner, B. T. McGuckin, R. T. Menzies, C. T. Bruegge, and V. Duval, "Directional-hemispherical reflectance for spectralon by integration of its bidirectional reflectance," *Appl. Opt.* **37**, 3996–3999 (1998).
19. P. Sperber and A. Penzkofer, " S_0 - S_n two-photon absorption dynamics of rhodamine dyes," *Opt. Quantum Electron.* **18**, 381–401 (1986).
20. D. A. Long, *Raman Spectroscopy* (McGraw-Hill, New York, 1977).
21. R. Loudon, *The Quantum Theory of Light* (Clarendon, Oxford, 1983).
22. D. P. Shelton, "Raman overtone intensities measured for H_2 ," *J. Chem. Phys.* **93**, 1491–1495 (1990).
23. D. M. Bishop and J. Pipin, "Calculated Raman overtone intensities for H_2 and D_2 ," *J. Chem. Phys.* **94**, 6073–6080 (1991).
24. E. W. Van Stryland and L. L. Chase, "Two-photon absorption: inorganic materials," in *CRC Handbook of Laser Science and Technology. Supplement 2: Optical Materials*, M. J. Weber, ed. (CRC, Boca Raton, Fla., 1995), pp. 299–328.
25. I. Shoji, T. Kondo, A. Kitamoto, M. Shirane, and R. Ito, "Absolute scale of second-order nonlinear-optical coefficients," *J. Opt. Soc. Am. B* **14**, 2268–2294 (1997).
26. D. A. Roberts, "Simplified characterization of uniaxial and biaxial nonlinear optical crystals: a plea for standardization of nomenclature and conventions," *IEEE J. Quantum Electron.* **28**, 2057–2074 (1992).
27. K. Hagimoto and A. Mito, "Determination of the second-order susceptibility of ammonium dihydrogen phosphate and α -quartz at 633 and 1064 nm," *Appl. Opt.* **34**, 8276–8282 (1995).
28. N. N. Vsevolodov, L. P. Kostikov, L. P. Kayushin, and V. I. Gorbatenkov, "Two-photon absorption of laser radiation by chlorophyll-a and certain organic dyes," *Biophysics (GB)* **18**, 807 (1973).
29. D. M. Bishop and J. Pipin, "Improved dynamic hyperpolarizabilities and field-gradient polarizabilities for helium," *J. Chem. Phys.* **91**, 3549–3551 (1989).
30. D. P. Shelton, "Nonlinear-optical susceptibilities of gases measured at 1064 and 1319 nm," *Phys. Rev. A* **42**, 2578–2592 (1990).
31. E. A. Donley and D. P. Shelton, "Hyperpolarizabilities measured for interacting molecular pairs," *Chem. Phys. Lett.* **215**, 156–162 (1993); "Erratum," **228**, 701 (1994).
32. D. P. Shelton and J. E. Rice, "Measurements and calculations of the hyperpolarizabilities of atoms and small molecules in the gas phase," *Chem. Rev.* **94**, 3–29 (1994).
33. R. J. Bartlett and H. Sekino, "Can quantum chemistry provide reliable molecular hyperpolarizabilities?" in *Nonlinear Optical Materials: Theory and Modeling*, S. P. Kama and A. T. Yeates, eds., ACS Symp. Ser. **628**, 23–57 (1996).
34. P. Norman, Y. Luo, D. Jonsson, H. Ågren, K. O. Sylvester-Hvid, and K. V. Mikkelsen, "Hyperpolarizability depolarization ratios of nitroanilines," *J. Chem. Phys.* **107**, 9063–9066 (1997).